Available online at www.sciencedirect.com

jmr&t Journal of Materials Research and Technology

journal homepage: www.elsevier.com/locate/jmrt

Original Article

Electrically conductive fibers fabrication and characterization via in-situ polymerization of aniline for the protection against EMI and thermal imaging signals

S Sadia Nimra [a,1], Z.A. Rehan [a], S Hasan Ali [a,1], Salman Atir [b], Kinza Fatima [c], Fatima Shahzadi [a], HM Fayzan Shakir [d,**], Mohammed A. Alamir [e], Tarek Mohamed Ahmed Ali EL-Bagory [f,g], Imran Shahid [h,*]

[a] Department of Materials, School of Engineering and Technology, National Textile University, Faisalabad, Pakistan
[b] College of Materials Science and Engineering, Nanjing University of Aeronautics and Astronautics, Nanjing, China
[c] Institute of Physics, The Islamia University of Bahawalpur, Bahawalpur, Pakistan
[d] NPU-NCP Joint International Research Center on Advanced Nanomaterials and Defects Engineering, Shaanxi Engineering Laboratory for Graphene New Carbon Materials and Applications, School of Materials Science and Engineering, Northwestern Polytechnical University, Xi'an, China
[e] Department of Mechanical Engineering, College of Engineering, Jazan University, Jazan 45142, Saudi Arabia
[f] Department of Mechanical and Industrial Engineering, College of Engineering, Majmaah University, Al-Majmaah, Riyadh 11952, Saudi Arabia
[g] Department of Mechanical Design, Faculty of Engineering Materia, Helwan University, Cairo 11724, Egypt
[h] Environmental Science Centre, PO Box 2713, Qatar University, Doha, Qatar

ARTICLE INFO

Article history:
Received 9 September 2022
Accepted 16 January 2023
Available online 26 January 2023

Keywords:
EMI shielding
DC conductivity
Polyester fibers
PANI
Fiber reinforced composites
Thermal imaging

ABSTRACT

Polyester fibers (PEF) were successfully coated with Polyaniline (PANI) via in situ polymerization to make electrically conductive fibers (ECF). X-ray diffraction (XRD) analysis confirms the synthesis and scanning electron microscopy (SEM) confirms the coating of PANI on the surface of PEF. Both coated and uncoated fibers were tested for their DC conductivity, and the results showed a clear difference between the two. From a highly insulating state, it transitions to about 0.1 S/cm. Both the tensile strength and modulus seemed to rise, going from 0.5 MPa to 2.5 MPa and from 0.04 MPa to 0.4 MPa, respectively. Blocking electromagnetic (EM) waves primarily requires a material with good electrical conductivity. The fabric proved effective in blocking about 99.9% of the ultraviolet (UV) and near-infrared rays. Fabrics that effectively block electromagnetic waves are able to conceal the high-temperature human body from a thermal imaging camera, which detects heat signatures by observing the infrared (IR) radiation generated by objects. We also measured the dielectric characteristics using impedance analysis and found that the values for the

* Corresponding author.
** Corresponding author.
E-mail addresses: Fayzan.shakir@mail.nwpu.edu.cn (H.F. Shakir), ishahid@qu.edu.qa (I. Shahid).
[1] Equal Contribution.

https://doi.org/10.1016/j.jmrt.2023.01.101

dielectric constant, dielectric loss, and AC conductivity dramatically increased from the frequency range of 100 Hz to 5 MHz. Further, electromagnetic interference (EMI) and shielding efficiency were determined with the aid of the dielectric constant and dielectric loss (SE). The overall SE in the same 100 Hz to 5 MHz range was similarly more than 80 dB. Improved EMI shielding was feasible due to the non-woven fabric's strong electrical conductivity, homogenous PANI coating on the surface, and great compactness. These findings are enough to predict that these fibers will provide good EMI shielding and thermal imaging when used in any application.

1. Introduction

The ability of thermal imaging cameras to detect human bodies is a major threat to soldiers at night. It's extremely difficult for the armed forces to conduct operations at night. Armed forces can use thermal imaging systems to detect temperature differences between extinct enemy forces and their surroundings [1–3]. Thermal imaging cameras use infrared radiation in the camera's field of vision and follow that information to produce a thermal image. As a result, EMI shielding is required for the army's protection against thermal imaging cameras, as well as for the internal armed suit's electrical systems from external radiations [4–7]. Over the last 20 years, the use of these gadgets has increased exponentially [8,9]. However, the major issue with the increased use of such electronic accessories is electromagnetic pollution. EMI shielding is presently one of the important issues for the defense of soldiers and technological gadgets. In this regard, polymer-based conductive composites have taken a tremendous amount of work to provide EMI shielding [10–12].

Now, conductive polymers are used for EMI shielding in several everyday applications, including aircraft, the military, energy, and electrical equipment. The conductive polymer-based EMI shielding helps us to protect electrical equipment (laptops, mobiles, sensitive sensors, electricity supply instruments, characterization devices, and so on). The use of conductive polymers has increased over the last two decades due to their versatility. This research has moved into the field of textiles with the goal of creating conductive fabrics for a variety of applications.

In past work, admicellar polymerization was used to prepare conductive polymer-coated fabrics. When a thin layer of the conductive polymers was coated on fabrics, an increase in the DC conductivity of the fabric was observed [13–16]. The study of polypyrrole/cotton composites reveals their high conductivity, flexibility, and thermal stability. Using an in situ polymerization technique, flexible polypyrrole/cotton textiles with a resistance of up to 0.37Ωcm can be produced [17–20]. Cotton fibers combined with polyaniline by in situ polymerization produce semi-conductive materials with a conductivity of almost (1.54×10^{-4} Scm^{-1}) [21–25]. Using polyaniline (PANI) and its settling on bagasse fiber (BF) (through the in situ polymerization of aniline in a dispersed system of BF), it was observed that the BF/PANI composite had a higher conductivity (2.01 ± 0.29 Scm^{-1}) than pristine PANI conductivity (1.35 ± 0.15 Scm^{-1}) [26–28]. A simple chemical polymerization approach has already been used to make a PANI nano-fibers composite with graphite. It has an EMI shielding of more than 80 dB in the frequency band (8.2–18) GHz with a thickness of 1 mm [29–32]. Polymers do not have a natural conductive characteristic. As a result, they are unable to provide enough protection for gadgets. According to the research, fillers are one of the items that have the potential to increase conductivity [7,33–35]. The study of polyacrylate expandable foam particles (PEFP) and nanoplatelets in (GNP) porous glass fiber mat indicated that by using GMT/PEFP/GNP-4.0 wt%, shielding can be easily obtained close to 33.8 dB with 22.8 MPa strength in conductive composites [36–38]. Insitu polymerization of barium hexaferrite-polypyrrole nanoparticles results in less than 1% transmission in the NIR region and less than −50dB shielding efficacy in the microwave range [39]. According to the examination of PVC-based composite files incorporating Ag/ZnS and PANI-Ag/ZnS nanoparticles the frequency of the PANI-ZnS nanoparticles reached 52.5 dB in 0.1–20 GHz. The transmission in the near-infrared range was estimated to be <0.5% [40–43].

In the current study, polyester fibers (PEF) were coated with polyaniline (PANI) to provide shielding against electromagnetic interference (EMI) and thermal imaging cameras (TIC). The in-situ polymerization method was used for the coating of electrically conductive PANI on PEF. The electrically conductive fibers (ECF) produced were characterized using DC conductivity, impedance, SEM, NIR spectroscopy, and mechanical properties. The major goal was to assess EMI shielding in the infrared area. For the hindering properties of IR, a wavelength of range 250–2500 nm was used. The results revealed that the shielding efficacy is more than 80 dB. According to IR spectroscopy, the composite sheets had less than 1% transmission throughout the whole NIR range.

2. Materials and methods

2.1. Materials

Formic acid (96%, Sigma Aldrich), Aniline monomer (99.5%, UNI CHEM chemical reagents), Ammonium persulfate (98%, DAE JUNG Korea), Polyester fibers (140 deniers, FARNA Textile, Pakistan), PVC (100%, Glory Plastic LTD) and THF (99.5%, DAE JUNG, Korea).

Table 1 – List of samples and their composition.

Sr#	Sample Names	Thickness
1	A1	1 mm (PEF)
2	A2	1 mm (ECF)
3	A3	1.5 mm (ECF)
4	A4	2 mm (ECF)

2.2. *Preparation of electrically conductive fibers (ECF)*

In-situ polymerization was adapted for the coating of PEF with PANI. A solution of APS (25 g) and aniline (25 ml) was prepared in formic acid (500 ml) separately at 50 °C at continuous stirring. Polyester fibers (25 g) were then added to an aniline solution and stirred for 1 h. After that, the beaker was set in an ice bath to achieve the desired polymerization temperature of 0–5 °C. APS solution was added dropwise to the aniline/fibers solution while maintaining a uniform temperature of 0–5 °C and continuously stirring. The dark greenish tint began to appear after some time. The solution was left for 2–3 h at continuous stirring to undergo complete polymerization. Afterward, the fibers were removed from the solution and washed with water and ethanol to remove unreacted APS, aniline, and excess formic acid content. It is then dried in a furnace overnight at 120 °C. For a better understanding, a flowchart is given below in Fig. 1. By using 15 g of PEF, 20 g of ECF was obtained. PSF/PANI wt ratio in ECF is 75:25.

2.3. *Fabrication of PANI-polyester composite*

A homogeneous solution of (15 g) PVC was made in (150 ml) of THF. PANI-coated fibers (15 g,30 g,45 g) were added to the PVC solution and left to soak. To let THF evaporate completely, the soaked fibers were spread evenly on an aluminum foil. The fibers were then placed on a Teflon sheet with a 6″ dimension. The Teflon sheet containing the fiber was placed in the compression molding machine at 80 °C temperature and 12-ton pressure. The composite sheets obtained were dried in a vacuum oven at 50 °C. Composites were made with different thicknes and shown in Table 1.

2.4. *Characterization*

2.4.1. *X-ray diffraction (XRD)*

X-ray analysis was done using 2θ from 10° to 70° with a stay duration of 1 s and a 0.02° increment. In this study, the D8 Discover of BRUKER company was utilized. In section 4.6, the results obtained are discussed.

2.4.2. *Scanning electron microscope (SEM)*

The "JEOL-instrument JSM-6490A" was utilized to examine the surface of PEF and ECF at different magnifications after coating with gold.

2.4.3. *DC conductivity*

The DC conductivity test was carried out using "Keithley 2450". The two probes were kept at a distance of 1 mm. After placing the probes, 5 V was applied and the current was measured using the ammeter. Further calculations for conductivity were done by utilizing the following relationship:

$$R = \frac{V}{I}, \rho = \frac{RA}{L}, \sigma = \frac{1}{\rho}$$

here R, V, and I represent resistance, voltage, and current, respectively. L and A denotes the length and area of the cross-section. Whereas ρ and σ represent the resistivity and value of conductivity, respectively.

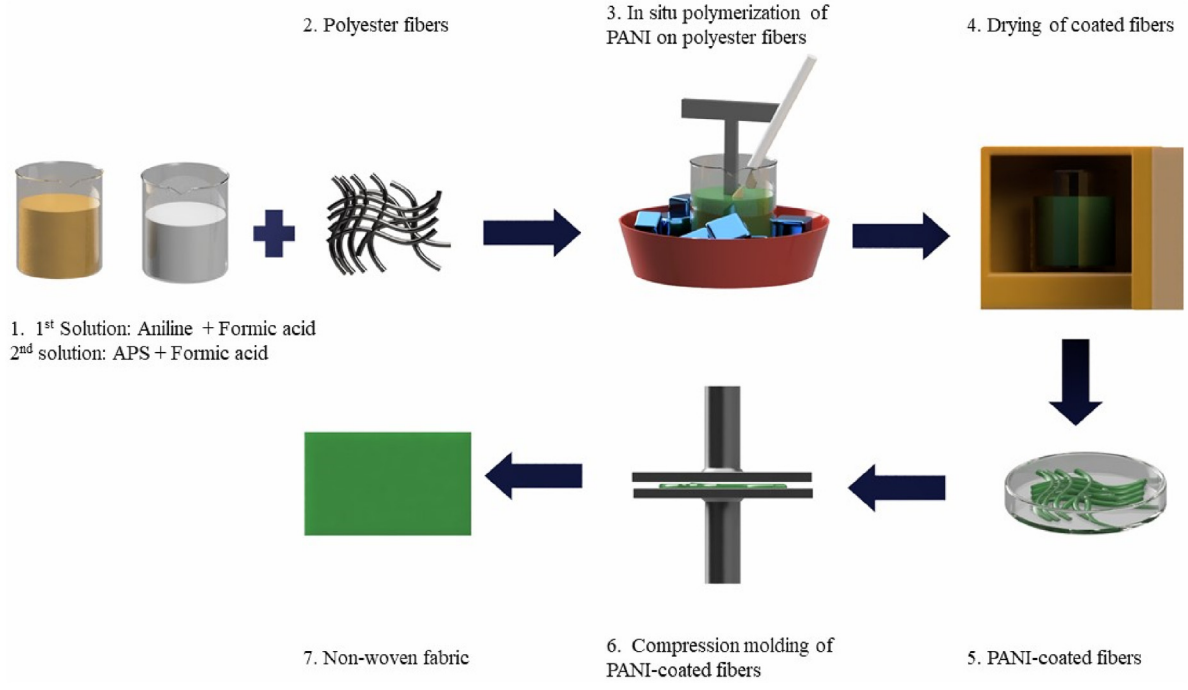

Fig. 1 – Visual representation of the experimental process.

2.4.4. *Mechanical properties*

Under ASTM standard D3039, the mechanical properties were evaluated using Ametek Lloyd's model LRX. The gauge length and width of the sample were 20 mm × 10 mm, and the strain rate was 1 mm/min.

2.4.5. *Impedance analyzer*

The "Wayne Kerr 6500B" was utilized to measure and determine impedance properties in the frequency range of 100 Hz to 5 MHz. The values of Tan δ and capacitance was obtained from it. The dielectric loss, AC conductivity, and dielectric constant were then determined using these data. Afterward, dielectric constant and loss parameters were used to calculate EMI shielding effectiveness in the same frequency region.

2.4.6. *Thermal imaging cameras*

Cantronic System Ins. IR916 captured the thermal images of non-woven fabric samples. The thermography camera uses an advanced 160x120 uncooled Microbolometer FPA detector to provide a radiometric 50/60 Hz real-time picture.

2.4.7. *IR spectroscopy*

"PerkinElmer's "Lambda 950″ was used to analyze the transmission of UV/Vis/NIR radiation through a composite sheet in the 250–2500 nm frequency range.

3. Result and discussion

3.1. *X-ray diffraction (XRD)*

PANI has a semi-crystalline structure and has two distinct peaks in its XRD pattern. PANI was synthesized using a chemical oxidative approach, and its success in creation was verified using x-ray diffraction. In Fig. 2, the XRD pattern of PEF and ECF is displayed. It is evident that PEF is completely amorphous as there is no prominent peak and only a rough and noisy graph. Whereas there are two peaks at $2\theta = 19^{\circ}$ and $2\theta = 25^{\circ}$ in the ECF pattern. These peaks arise from periodicity horizontal and vertical periodicity of the polymer chain. A similar XRD pattern of XRD also reported by Khadija et al. [44].

3.2. *Scanning electron microscopy (SEM)*

The structural investigation of the nanocomposite was done using scanning electron microscopy. PEF and ECF were coated with gold and their surface features were observed at different magnifications. In Fig. 3 a and b, low-resolution images of both PEF and ECF was shown. It can be seen that PEF has a very smooth surface with no visible discontinuities or flaws. The rough surface of the ECF verifies the binding of polyaniline nanoparticles to the fiber surface. In the high-resolution image (Fig. 3c) the nanoparticles attached can be clearly seen and it is quite homogeneous. It can be expected from the SEM micrographs that fibers became electrically conductive and later on verified by DC conductivity measurement in section 3.3. Polyaniline was decorated on the surface of carbon fibers by Weiwei et al. and got similar SEM micrographs [45]. The PANI nanoparticles content was measured in weight percentage, after in situ polymerization and drying of fibers.

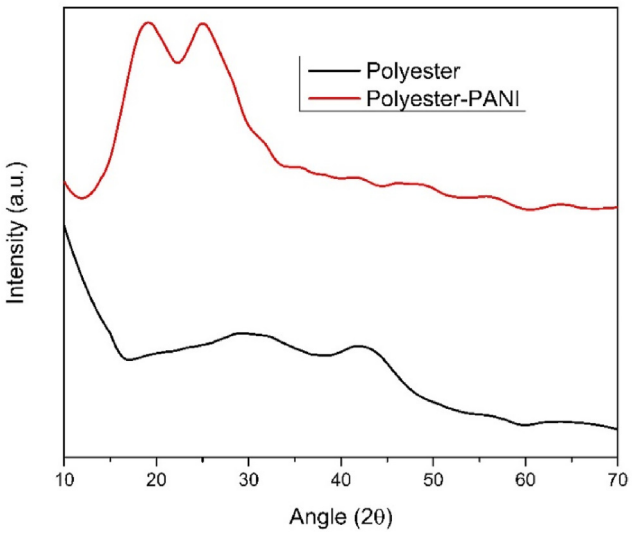

Fig. 2 – XRD of the prepared sample.

The comparison between the weight of pure polyester fibers and the weight after the coating of fibers gives information that the coated fibers contain 25 wt % of PANI Nano particles content.

3.3. *DC conductivity*

DC conductivity of samples A1 and A2 was measured by the 4-probe technique. Samples were cut in the dimensions of 5 mm * 10 mm The obtained DC conductivity values after calculations are shown in Fig. 4. Sample A1 exhibits a conductivity of 1.5×10^{-13} S/cm which is an insulative region. As the PANI is coated on insulated PEF, a significant increase in conductivity can be seen. This prominent change in conductivity value was due to the pi-electrons in the PANI structure. The conductivity value increases as a result of the formation of a densely interconnected network structure.

3.4. *Mechanical properties*

ASTM D3039 standard samples were cut with the dimension of 20 mm gauge length and 10 mm width. The strain rate of 1 mm/min was used for the measurement. Three samples were tested for each fabric sample and the average results are shown in Fig. 5. The standard deviation of data obtained for each sample is almost 3%. Through the stress-strain curve, the Ultimate tensile strength, elongation at break, and modulus of each sample for a constant value of strain i.e., 10% were compared. Samples started to break and cracks appeared at UTM (shown in Figure a) and rupture at the maximum elongation point. For sample A1, UTS was about only 0.35 MPa. By adding PANI and increasing fabric GSM in samples A2 and A3, the stress value increased to 24 and 2.3 respectively. The stress value again dropped to 0.35 because of the high amount of fibers and the same amount of binder. On the other hand, elongation at break decreased from sample A2 to A3 and then increased again for A4. Because there is no PANI

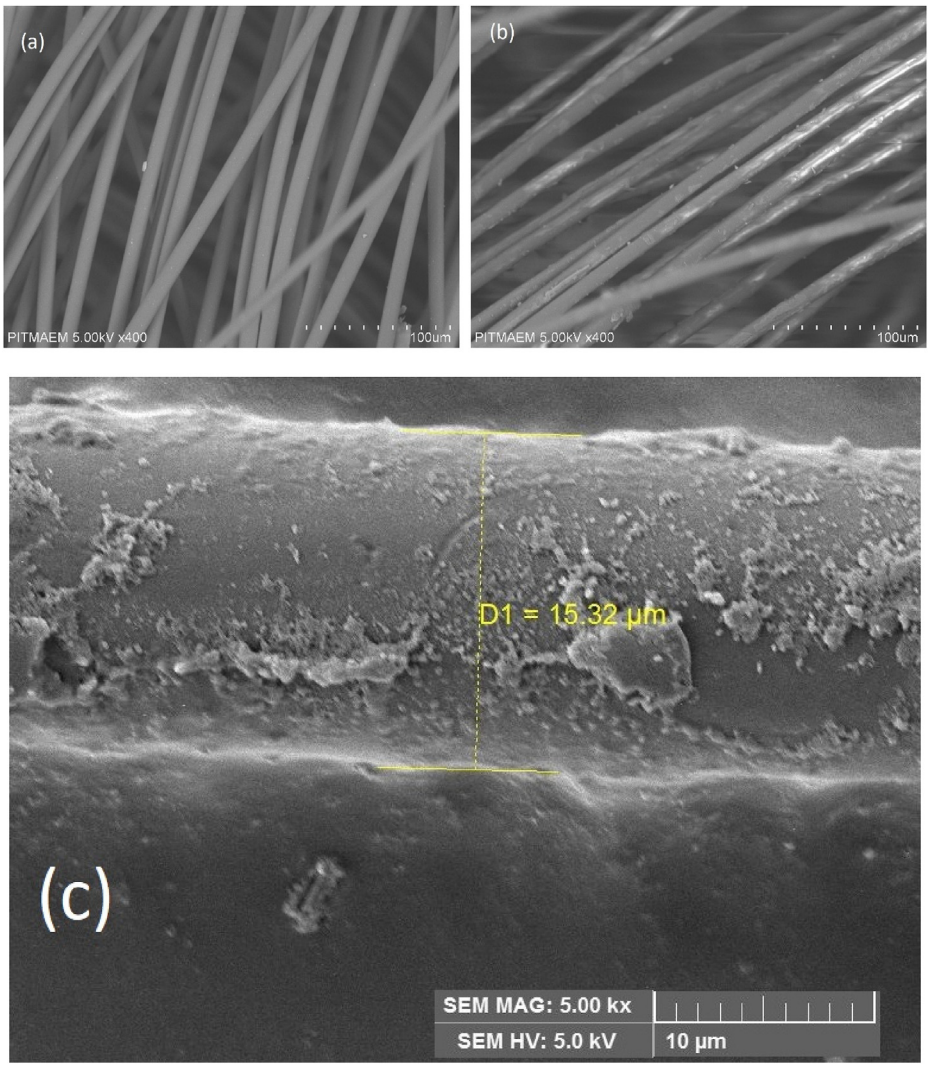

Fig. 3 – SEM images of different samples (a) PSF (b) ECF at low resolution and (c) ECF at high resolution.

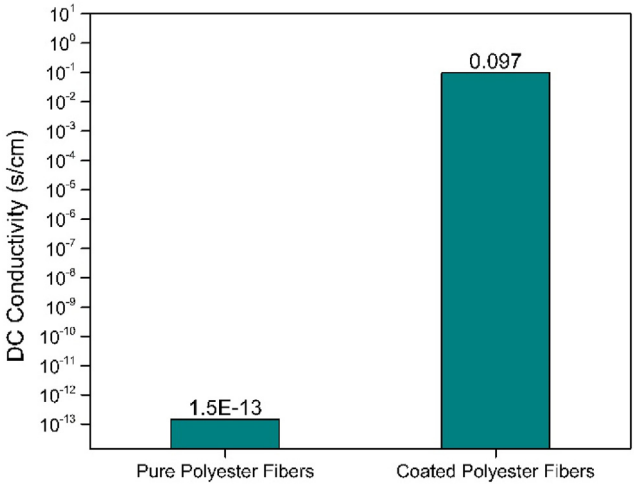

Fig. 4 – DC conductivity of the prepared samples.

reinforcement, A1's modulus is very low. As PANI is added in A2 and a high concentration of binder, the maximum modulus was achieved. From A2 to A4, the number of fibers increased with a constant amount of binder.

3.5. *Dielectric properties*

Dissipation factor (tan δ) and capacitance (C) from 100 Hz to 5 MHz were measured by an impedance analyzer (Wayne Kerr 6500B). Dielectric constant (Ɛ′), dielectric loss (Ɛ″), and AC conductivity (σ_{ac}) were determined using the following relationships and shown in Fig. 6:

$$Ɛ' = \frac{Cd}{AƐo}, Ɛ'' = \text{Tan}\,\delta * Ɛ',\ \sigma_{ac} = \omega\, Ɛo\, Ɛ'\, \tan\delta$$

here C, d, and A are the capacitance, thickness, and area of the sample. Whereas Ɛo and ω are the permittivity of free space and angular frequency.

The dielectric constant enables us to know the amount of charge that can be stored at one time. The result shows that by

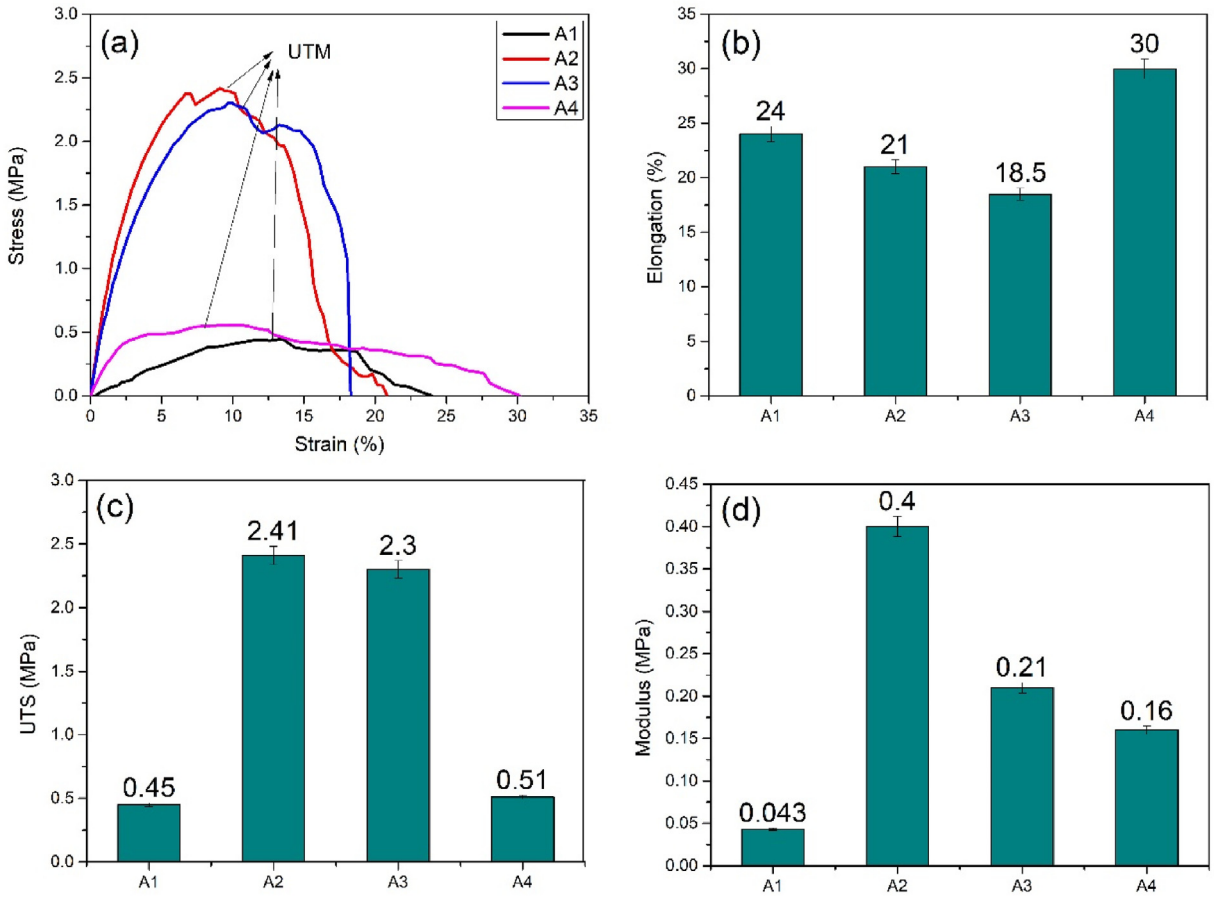

Fig. 5 – Mechanical properties of prepared nanocomposite sheet.

increasing the thickness of the polyester fabric and filler amount, the dielectric constant value increases. A1 shows the lowest dielectric constant as it contains PEF with no free electrons. The sample A2 has a marginally higher dielectric constant due to the presence of conductive PANI, whereas sample A3 has a higher dielectric constant value as the thickness increases. Sample A4 has the highest number of free electrons due to the fact that it shows the highest dielectric constant value compared to samples A1, A2, and A3. Fig. 8a shows the graphical results of the dielectric constant. Enhanced dielectric constant values of PANI have already been reported by Khadija et al. [44].

Whenever an electric field is altered, some of the energy is lost to reorient the dipole in opposite directions and termed dielectric loss. The dielectric loss also follows the same behavior as the dielectric constant. The pure sample A1 shows the lowest dielectric loss value as there are almost no dipoles to orient and reorient in opposite direction, while the sample A2 due to the availability of dipoles in PANI shows a marginally increased dielectric loss value. As the thickness of the fabric goes up in sample A3, the dielectric loss goes up, but sample A4 has the highest dielectric loss because it has the most electric dipoles.

The AC conductivity of samples doesn't change as much when the thickness of the samples is changed, but it does change when the frequency is changed. The sample A1 and A2 and A3 express almost the same AC conductivity. The frequency effect is only prominent in sample A4 and increases as the frequency increases. The overall behavior of the AC conductivity of samples is given in Fig. 6.

3.6. *Thermal imaging*

In order to investigate how IR radiations are blocked, thermal images of all samples were tested with a thermal imaging camera. In thermal imaging cameras, the IR waves are gathered and converted to electrical signals. Afterward, the signals are displayed in the form of colors which signify the values of temperature. Fig. 7 displays the thermal images of all the samples. The Pure sample A1 showed the lightest shade which implied that it has a maximum transmission and minimal absorption of IR radiations. The reason behind the lightest shade of sample A1 is the absence of conductive PANI nanoparticles. From samples A2 to A4, the absorption was increased due to the addition of conductive PANI and the increased fabric thickness. The sample A4 showed the darkest shade as compared to other fabric samples, because sample A4 fabric has the highest thickness with the most number of conductive fibers. So from thermal imaging results, It can be concluded that with the addition of conductive material the absorption of the IR radiations is increased. Rukhsar et al. [46] and sabahat et al. [47] used PANI, Polyaniline and showed a

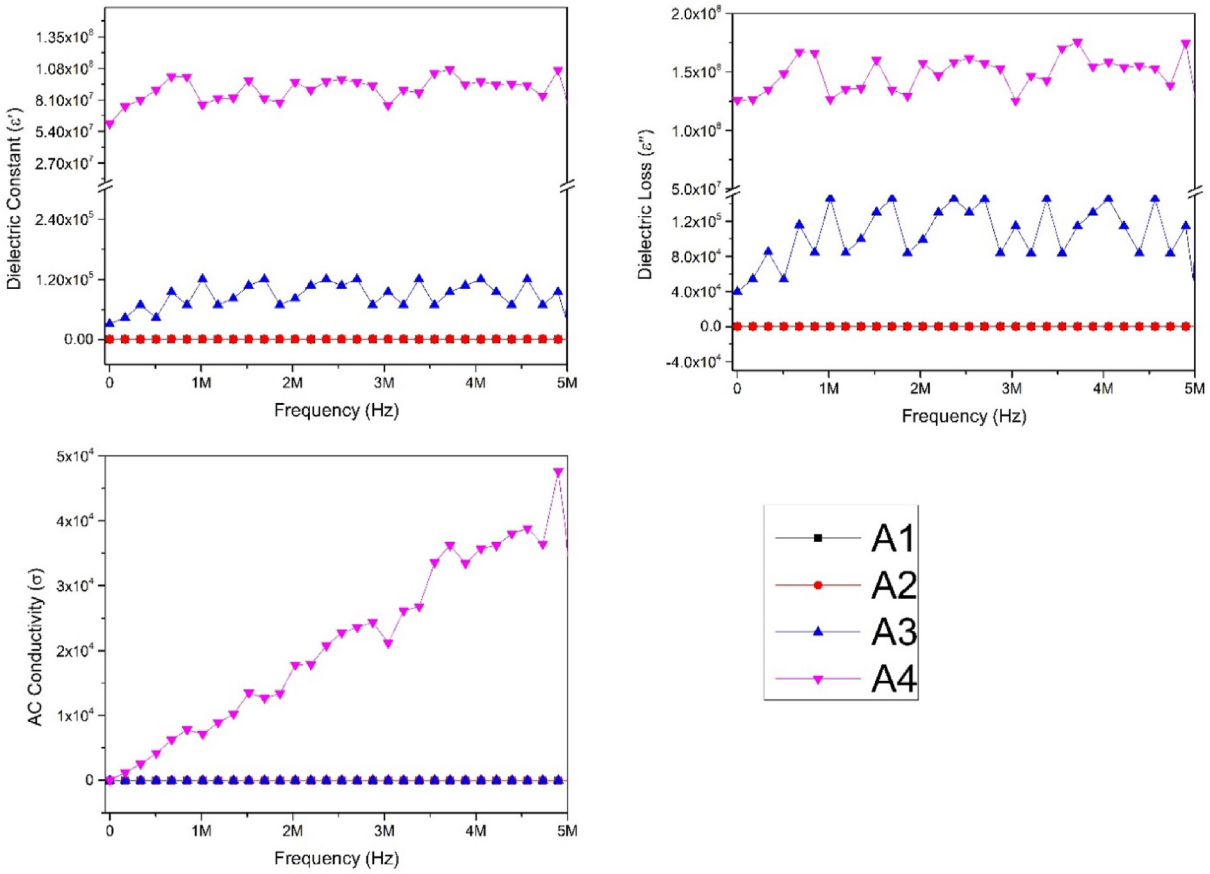

Fig. 6 – Dielectric constant, dielectric loss, and AC conductivity of the samples.

similar pattern of thermal images. With the addition of conductive filler, IR radiation is blocked by the PVC-based film.

3.7. *IR spectroscopy*

As previously stated in Section 3.6, the fabric completely blocked IR radiations; this was confirmed by UV/Vis/NIR spectroscopy as well as in the different spectra. The nanocomposite sheet was cut according to the sample holder size which is 10 mm in width and 30 mm in length. Radiation transmission was measured in the UV/VIS/NIR region from 200 to 2500 nm. The sample A1 shows almost 80% transmission. With the addition of aniline content, the transmission of IR radiations reduced to less than 0.5%. All the obtained data of transmission is shown in Fig. 8. Due to the good dispersion of aniline and conductive networked structure all the radiation was hindered. From the results it can be concluded that the electrically conductive structure effectively blocked the greatest quantity of IR radiations and preventing their passage from fabric.

3.8. *EMI shielding*

The impedance analyzer was used to determine the capacitance and dissipation factors in the frequency region of 100 Hz to 5 MHz Dielectric constant, dielectric Loss and AC conductivity was already calculated in section 3.5. By using the following relationships, SER SEA and SET were then calculated and shown in Fig. 9.

$$SE_A = 8.8\ \alpha l$$

$$SE_R = 20 \log \frac{|1+n|^2}{4n}$$

$$\alpha = \frac{2\pi}{\lambda}\sqrt{\frac{\varepsilon'\sqrt{1+tan^2\,\delta}}{2}}$$

$$n = \sqrt{\frac{\varepsilon'\sqrt{1+tan^2\,\delta}+1}{2}} + i\sqrt{\frac{\varepsilon'\sqrt{1+tan^2\,\delta}+1}{2}}$$

When electromagnetic radiation (EMR) comes into contact with matter, the EM wave is reflected, absorbed, and transmitted, as postulated by the EMI theory. Three methods exist for shielding against electromagnetic interference that are absorption (SE_A), multiple reflections (SE_{MR}), and reflection (SE_R). If the overall efficiency of the shielding is more than 10 dB, then the SE_{MR} is often disregarded, and no calculations are required. The combined efficacy of the remaining two shielding processes is given by Refs. [8,48]:

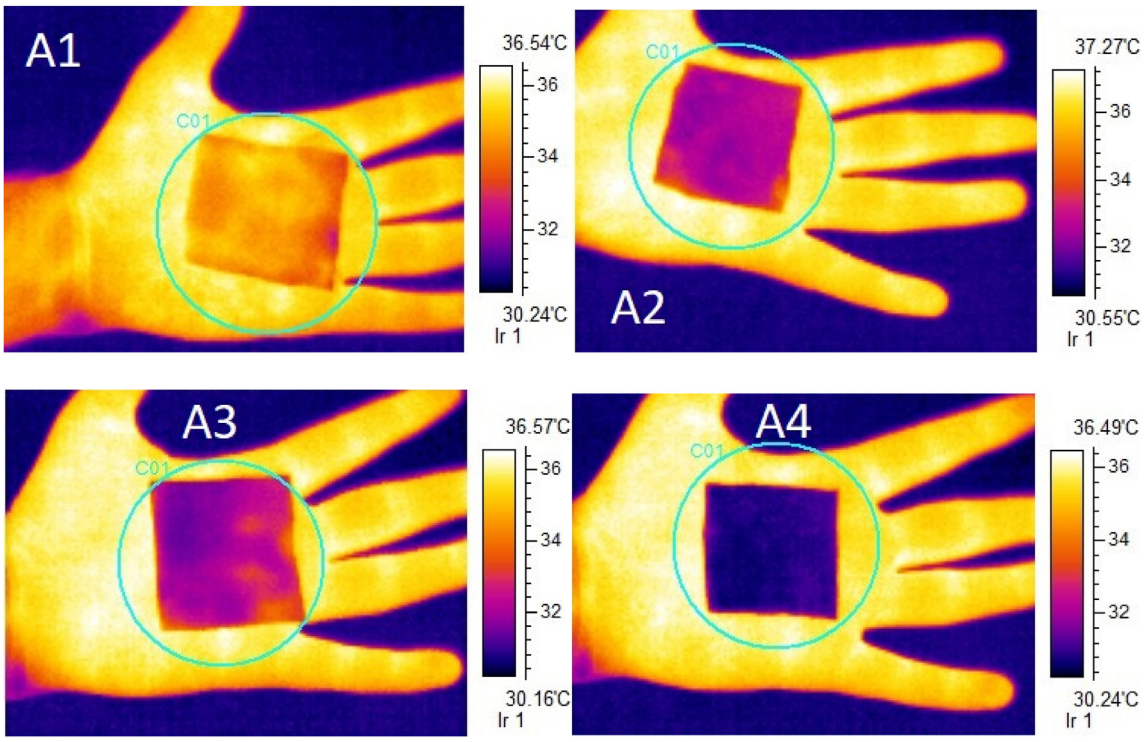

Fig. 7 – Thermal images of the prepared sample.

$$SE_T = SE_A + SE_R = \log\frac{EIN}{EOUT}$$

The study regarding the method of absorption (SE_A) gives information that the frequency of electromagnetic radiation effects the absorption behavior of samples with respect to the number of PANI-coated fibers and fabric thickness. The fabric samples A1 and A2 exhibit the same behavior by absorbing the lowest amount of radiation by increasing frequency; the reason is that both samples A1 and A2 have a minimum thickness. The other reason is that sample A1 contains pure fibers and sample A2 has a low number of PANI-coated fibers. The sample A3 has a higher number of PANI-coated fibers than A1 and A2, and due to this fact, it exhibits a slight change in the absorption of radiation, as frequency has essentially little effect on the absorption behavior. According to the preceding discussion, samples A1, A2, and A3 have low absorption values. However, when the frequency of the electromagnetic radiation rises, the sample's absorption

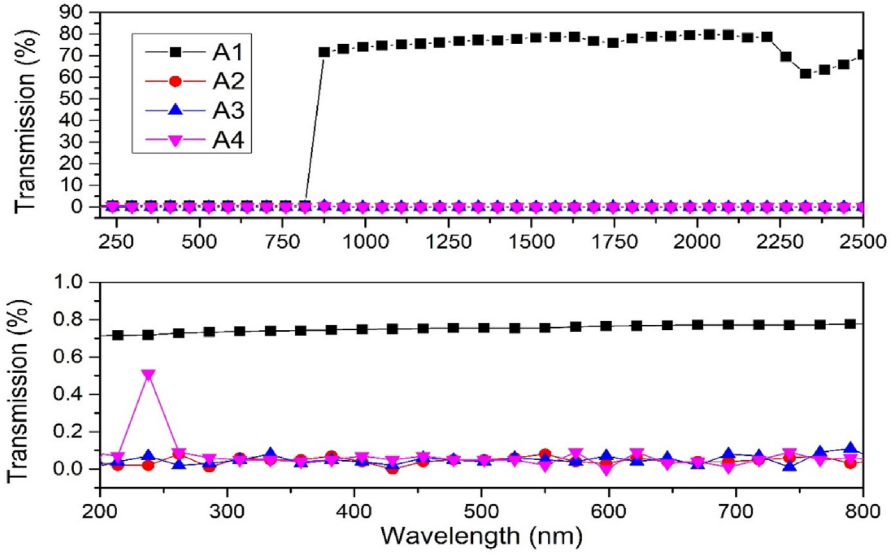

Fig. 8 – UV/VIS/NIR transmission.

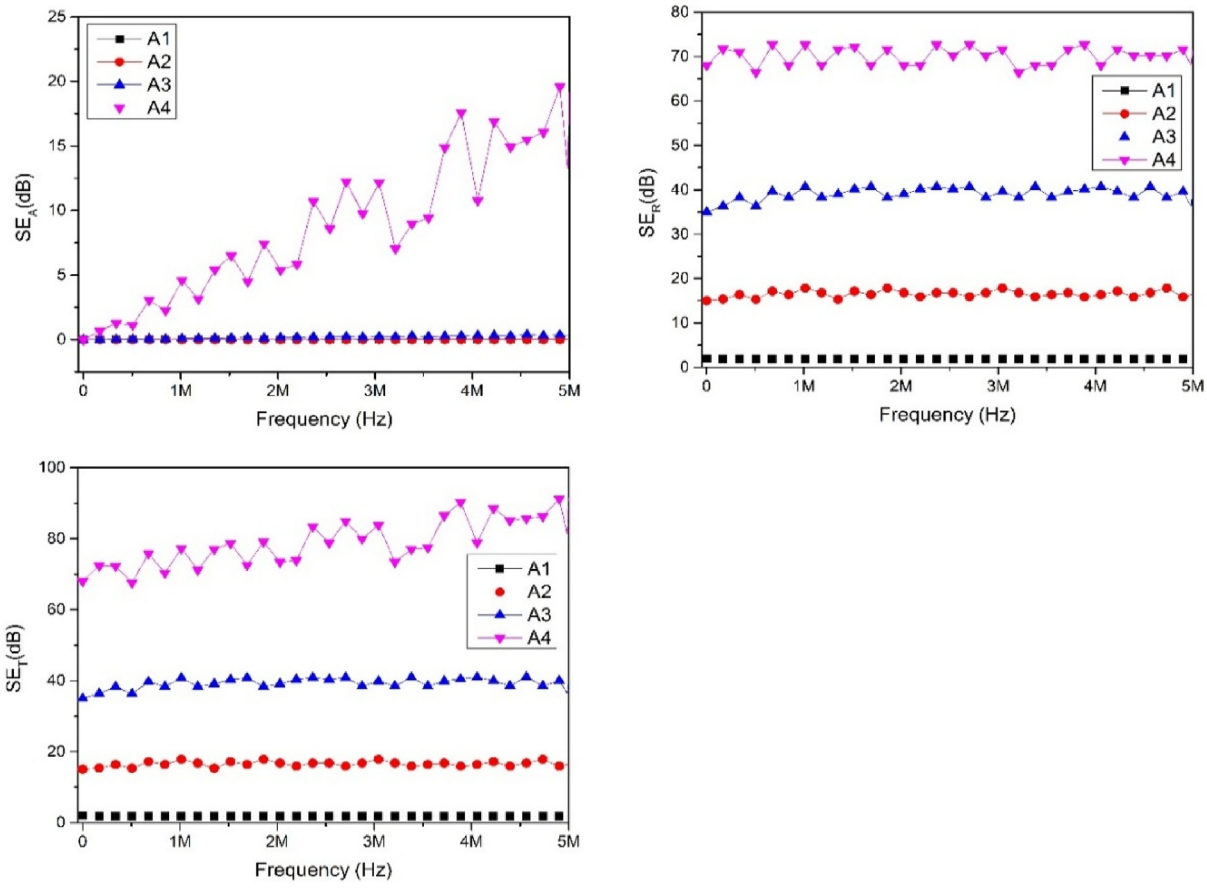

Fig. 9 – SE_A, SE_R, and SE_T of samples.

behavior increases. The reason is that the increasing frequency exhibits a high effect on the absorption of sample A4 fabric, which has the highest number of PANI-coated fibers and thickness as well.

The reflection study reveals that electromagnetic radiation reflection increases as the thickness of the fabric sample increases. Pure sample A1 doesn't have any PANI-coated fibers due to this it reflects less electromagnetic radiation than sample A2, which contains PANI-coated fibers. The samples A3 and A4 show an increase in reflection as the thickness increases with an increase in the amount of coated fibers in the fabric sample, respectively. The sample A4 shows exceptional shielding with the highest reflection of electromagnetic radiation because this sample has highest thickness. The overall reflection behavior of radiations in samples is given in Fig. 9.

The transmission (SE_T) behavior study of the samples gives the information that transmission decreases as the thickness of the coated sample increases. Sample A1 has a non-conductive structure due to this, it exhibits a high transmission of electromagnetic radiation. In sample A2, there is less transmission of electromagnetic radiation as compared to sample A1 because PANI-coated fibers are present. The results give sense that with the presence of conductive structure, if the thickness of the fabric samples goes up than the high amount of transmission will stop. Similarly, the sample A3 blocks a good amount of electromagnetic radiation because its thickness is higher than that of the sample A1 and the sample A2. The Sample A4 has a best shielding by blocking the most electromagnetic radiation because its thickness is highest in all fabric samples.

The EMI shielding increases as the shielding effectiveness increases. Everyone is aware that the shielding effectiveness is determined by the PANI content. This content was measured as a percentage of the weight on the surface of polyester fibers, as previously stated. For this, the weight of polyester fibers before and after the in situ polymerization was calculated. After the comparison of the weights, the difference between the pure polyester fibers and coated polyester fibers is assumed to be the weight content of the PANI on the fibers. The content of PANI was optimized by increasing the thickness of fabric sheet. The thicker polyester fabric sheet contains more coated fibers in compact form, which means these fabric sheets have more PANI content, and that's why these thicker samples have shown greater shielding effectiveness.

4. Conclusion

Polyester fibers (PEF) were successfully coated with Polyaniline (PANI) via in situ polymerization to make electrically

conductive fibers (ECF). XRD analysis confirms the synthesis and SEM confirms the coating of PANI on the surface of PEF. Almost 0.1 S/cm of DC conductivity was observed that also proves the fabrication of ECF. Non-woven fabric was prepared using PVC as a binder via compression molding. Both mechanical and dielectric properties seemed to increase with the increase in the thickness of the fabric. UV/Vis/NIR spectroscopy and thermal imaging signal analysis exhibit 99.9% blockage of waves falling in the mentioned spectrum. EMI shielding in 100 Hz to 5 MHz frequency region was calculated. More than 70 dB shielding effectiveness in the whole frequency region of 100 Hz to 5 MHz. Which is enough to predict that these fibers will give good EMI shielding and thermal imaging when used in concerned application.

Declaration of Competing Interest

The authors declare that they have no known competing financial interests or personal relationships that could have appeared to influence the work reported in this paper.

REFERENCES

[1] Szajewska A. Development of the thermal imaging camera (TIC) technology. Procedia Eng 2017;172:1067–72. https://doi.org/10.1016/j.proeng.2017.02.164.

[2] Berg A. Detection and tracking in thermal infrared imagery. 2016. p. 1744. https://doi.org/10.3384/lic.diva-126955.

[3] Ratches JA, Chait R, Lyons JW. Some recent sensor-related army critical technology events. Def. Technol. Pap. 2013;1(1):35.

[4] Gulzar N, Zubair K, Shakir MF, Zahid M, Nawab Y, Rehan ZA. Effect on the EMI shielding properties of cobalt ferrites and coal-fly-ash based polymer nanocomposites. J Supercond Nov Magnetism 2020. https://doi.org/10.1007/s10948-020-05608-w.

[5] Shakir MF, et al. EMI shielding properties of polymer blends with inclusion of graphene nano platelets. Results Phys 2019;14(May):102365. https://doi.org/10.1016/j.rinp.2019.102365.

[6] Liu R, Wang D, Xie Y, Li J, Wang L. Flexible cellulose-based material with a higher conductivity and electromagnetic shielding performance from electroless nickel plating. Wood Sci Technol 2021;55(6):1693–710. https://doi.org/10.1007/s00226-021-01297-3.

[7] Subramanian J, Kumar SV, Venkatachalam G, Gupta M, Singh R. An investigation of EMI shielding effectiveness of organic polyurethane composite reinforced with MWCNT-CuO-bamboo charcoal nanoparticles. J Electron Mater 2021. https://doi.org/10.1007/s11664-020-08622-9.

[8] Zubair K, et al. Study of mechanical, electrical and EMI shielding properties of polymer-based nanocomposites incorporating polyaniline coated graphene nanoparticles. Nano Express 2021;2(1):010038. https://doi.org/10.1088/2632-959x/abe843.

[9] Zubair K, Shakir MF, Afzal A, Rehan ZA, Nawab Y. Effect of barium hexaferrites and thermally reduced graphene oxide on EMI shielding properties in polymer composites. J Supercond Nov Magnetism 2020. https://doi.org/10.1007/s10948-020-05669-x.

[10] Networks N, Park S, Ha J. Properties Through the Use of Segregate Carbon 2019:6–13.

[11] Sankaran S, Deshmukh K, Ahamed MB, Pasha SKK. Recent advances in electromagnetic interference shielding properties of metal and carbon filler reinforced flexible polymer composites : a review. Compos Part A 2018. https://doi.org/10.1016/j.compositesa.2018.08.006.

[12] Xia X, Xiao Q. Electromagnetic interference shielding of 2d transition metal carbide (Mxene)/metal ion composites. Nanomaterials 2021;11(11). https://doi.org/10.3390/nano11112929.

[13] Lekpittaya P, Yanumet N, Grady BP, Rear EAO. Resistivity of Conductive Polymer – Coated Fabric 2003:2–9.

[14] Collins GE, Buckley LJ. Conductive polymer-coated fabrics for chemical sensing. Synth Met 1996;78(2):93–101. https://doi.org/10.1016/0379-6779(96)80108-1.

[15] Takamatsu S, Imai T, Yamashita T, Kobayashi T, Miyake K, Itoh T. Flexible fabric keyboard with conductive polymer-coated fibers. Proc IEEE Sensors 2011:659–62. https://doi.org/10.1109/ICSENS.2011.6127391.

[16] Maity S, Chatterjee A. Conductive polymer-based electro-conductive textile composites for electromagnetic interference shielding. A review 2016;47(8):2228–2252, Sep. https://doi.org/10.1177/1528083716670310. 10.1177/1528083716670310.

[17] Xie J, Pan W, Guo Z, Jiao SS, Ping Yang L. In situ polymerization of polypyrrole on cotton fabrics as flexible electrothermal materials. J. Eng. Fiber. Fabr. 2019;14. https://doi.org/10.1177/1558925019827447.

[18] Zou Y, Reddy N, Yang Y. Reusing polyester/cotton blend fabrics for composites. Compos B Eng Jun. 2011;42(4):763–70. https://doi.org/10.1016/J.COMPOSITESB.2011.01.022.

[19] Paiva Júnior CZ, De Carvalho LH, Fonseca VM, Monteiro SN, D'Almeida JRM. Analysis of the tensile strength of polyester/hybrid ramie–cotton fabric composites. Polym Test 2004;23(2):131–5. https://doi.org/10.1016/S0142-9418(03)00071-0.

[20] Hashmi SAR, Dwivedi UK, Chand N. Graphite modified cotton fiber reinforced polyester composites under sliding wear conditions. Wear May 2007;262(11–12):1426–32. https://doi.org/10.1016/J.WEAR.2007.01.014.

[21] Teklu T, et al. Polyaniline deposition on the surface of cotton fibers: structural studies, swelling behavior, and water absorption properties. Adv Mater Sci Eng 2020;2020. https://doi.org/10.1155/2020/1650364.

[22] SID.Ir | conductivity of textile fibers treated with aniline."

[23] Li R, Liu G, Gu F, Wang Z, Song Y, Wang J. In situ polymerization of aniline on acrylamide grafted cotton. J Appl Polym Sci 2011;120(2):1126–1132, Apr. https://doi.org/10.1002/APP.30388.

[24] Su J, et al. Conductive cotton by in situ laccase-polymerization of aniline. Polym 2018;10(9):1023. https://doi.org/10.3390/POLYM10091023. 2018.

[25] Gao D, et al. Polyaniline/silver nanowire cotton fiber: a flexible electrode material for supercapacitor. Adv Powder Technol 2021;32(11):3954–63. https://doi.org/10.1016/J.APT.2021.08.019.

[26] Zhang Y, Qiu M, Yu Y, Wen B, Cheng L. A Novel polyaniline-coated bagasse fiber composite with core-shell heterostructure provides effective electromagnetic shielding performance. ACS Appl Mater Interfaces 2017;9(1):809–18. https://doi.org/10.1021/acsami.6b11989.

[27] Zhang Y, Yang Z, Yu Y, Wen B, Liu Y, Qiu M. Tunable electromagnetic interference shielding ability in a one-dimensional bagasse fiber/polyaniline heterostructure. ACS Appl Polym Mater 2019;1(4):737–45. https://doi.org/10.1021/acsapm.8b00025.

[28] Shah BA, Abebe AA, Shah AV. Microwave-synthesized barium-impregnated siliceous zeolitic material derived from

bagasse fly ash for uptake of aniline. 2016 Arab J Sci Eng 2016;42(1):139–52. https://doi.org/10.1007/S13369-016-2083-9. 421.
[29] Joseph N, Varghese J, Sebastian MT. In situ polymerized polyaniline nanofiber-based functional cotton and nylon fabrics as millimeter-wave absorbers. Polym J 2017;49(4):391–9. https://doi.org/10.1038/pj.2016.121.
[30] Nayak R, Shetty P, Rao SM,A, Rao KM. Formulation of new screen printable PANI and PANI/Graphite based inks. Printing and characterization of flexible thermoelectric generators," Energy 2022;238:121680. https://doi.org/10.1016/J.ENERGY.2021.121680.
[31] Mashkour M, Rahimnejad M, Mashkour M. Bacterial cellulose-polyaniline nano-biocomposite: a porous media hydrogel bioanode enhancing the performance of microbial fuel cell. J Power Sources Sep. 2016;325:322–8. https://doi.org/10.1016/J.JPOWSOUR.2016.06.063.
[32] El-Basaty AB, Moustafa E, Fouda AN, El-Moneim AA. 3D hierarchical graphene/CNT with interfacial polymerized polyaniline nano-fibers. Spectrochim Acta Part A Mol Biomol Spectrosc 2020;226:117629. https://doi.org/10.1016/J.SAA.2019.117629.
[33] Kruželák J, Kvasničáková A, Hložeková K, Hudec I. Progress in polymers and polymer composites used as efficient materials for EMI shielding. Nanoscale Adv 2021;3(1):123–72. https://doi.org/10.1039/d0na00760a.
[34] Singh SK, Akhtar MJ, Kar KK. Hierarchical carbon nanotube-coated carbon fiber: ultra lightweight, thin, and highly efficient microwave absorber. ACS Appl Mater Interfaces 2018;10(29):24816–28. https://doi.org/10.1021/acsami.8b06673.
[35] Wang G, Zhao J, Ge C, Zhao G, Park CB. Nanocellular poly(ether-block-amide)/MWCNT nanocomposite films fabricated by stretching-assisted microcellular foaming for high-performance EMI shielding applications. J Mater Chem C 2021;9(4):1245–58. https://doi.org/10.1039/d0tc04099a.
[36] Ma M, et al. Lightweight and high-strength GMT/PEFP/GNP composites with absorb-dominated electromagnetic interference shielding property. J Mater Sci Mater Electron 2021;32(21):25863–75. https://doi.org/10.1007/s10854-020-04970-8.
[37] Zahid M, et al. M-type barium hexaferrite-based nanocomposites for EMI shielding application: a review. J Supercond Nov Magnetism 2021;34(4):1019–45. https://doi.org/10.1007/s10948-021-05859-1.
[38] Yang X, et al. Synchronously improved electromagnetic interference shielding and thermal conductivity for epoxy nanocomposites by constructing 3D copper nanowires/thermally annealed graphene aerogel framework. Compos. Part A Appl Sci Manuf 2020;128:105670. https://doi.org/10.1016/j.compositesa.2019.105670. June 2019.
[39] Shakir HF, et al. In-situ polymerization and EMI shielding property of barium hexaferrite/pyrrole nanocomposite. J Alloys Compd 2022;902:163847. https://doi.org/10.1016/j.jallcom.2022.163847.
[40] Zahid M, Shakir HF, Rehan ZA. Electromagnetic interference shielding study in microwave and NIR regions by highly efficient Ag/ZnS and polyaniline-Ag/ZnS particles. J Thermoplast Compos Mater 2021:1–15. https://doi.org/10.1177/08927057211064990.
[41] Dutta K, Manna S, De SK. Optical and electrical characterizations of ZnS nanoparticles embedded in conducting polymer. Synth Met Feb. 2009;159(3–4):315–9. https://doi.org/10.1016/J.SYNTHMET.2008.09.003.
[42] Bompilwar SD, Kondawar SB, Tabhane VA, Kargirwar SR. Thermal stability of CdS/ZnS nanoparticles embedded conducting polyaniline nanocomposites. Pelagia Res Libr Adv Appl Sci Res 2010;1(1):166–73.
[43] Chang CJ, Chu KW. ZnS/polyaniline composites with improved dispersing stability and high photocatalytic hydrogen production activity. Int J Hydrogen Energy 2016;41(46):21764–73. https://doi.org/10.1016/J.IJHYDENE.2016.07.155.
[44] Zubair K, et al. Study of mechanical, electrical and EMI shielding properties of polymer-based nanocomposites incorporating polyaniline coated graphene nanoparticles. Nano Express 2021;2(1) [Online]. Available: http://iopscience.iop.org/article/10.1088/2632-959X/abe843.
[45] Kong W, et al. Polyaniline-decorated carbon fibers for enhanced mechanical and electromagnetic interference shielding performances of epoxy composites. Mater Des 2022;217:110658. https://doi.org/10.1016/j.matdes.2022.110658.
[46] Anum R, Zahid M, Siddique S, Shakir HF, Rehan Z. PVC based flexible nanocomposites with the incorporation of Polyaniline and Barium Hexa-Ferrite nanoparticles for the shielding against EMI, NIR, and thermal imaging cameras. Synth. Met.; 2021. https://doi.org/10.1016/j.synthmet.2021.116773 [Online]. Available:.
[47] Siddique S, Zahid M, Anum R, Shakir HF, Rehan Z. Fabrication and characterization of PVC based flexible nanocomposites for the shielding against EMI, NIR, and thermal imaging signals. Results Phys.; 2021.
[48] Shakir MF, et al. EMI shielding characteristics of electrically conductive polymer blends of PS/PANI in microwave and IR region. J Electron Mater 2019. https://doi.org/10.1007/s11664-019-07631-7.